Chemokines form complex signals during inflammation and disease that can be decoded by extracellular matrix proteoglycans

Authors: Amanda JL Ridley[1], Yaqing Ou[1], Richard Karlsson[2], Nabina Pun[1], Holly L Birchenough[1], Thomas A Jowitt[1], Craig Lawless[1], Rebecca L Miller[2] and Douglas P Dyer[1,3].

Affiliations:

[1] Wellcome Centre for Cell-Matrix Research, Lydia Becker Institute of Immunology and Inflammation, Faculty of Biology, Medicine and Health, Manchester Academic Health Science Centre, University of Manchester, United Kingdom

[2] Copenhagen Center for Glycomics, Department of Cellular and Molecular Medicine, Faculty of Health Sciences, University of Copenhagen, Blegdamsvej 3, DK-2200 Copenhagen N, Denmark

[3] Geoffrey Jefferson Brain Research Centre, Manchester Academic Health Science Centre, Northern Care Alliance NHS Group, University of Manchester, Manchester, UK

Abstract

Chemokine driven leukocyte recruitment is a key component of the immune response and is central to a wide range of diseases. However, there has yet to be a clinically successful therapeutic approach that targets the chemokine system during inflammatory disease; possibly due to the supposed redundancy of the chemokine system. A range of recent studies have demonstrated that the chemokine system is in fact based on specificity of function. Here we have generated a resource to analyse chemokine gene (ligand and receptor) expression across

different species, tissues and diseases; revealing complex expression patterns whereby multiple chemokine ligands that mediate recruitment of the same leukocyte type are expressed in the same context, e.g. the CXCR3 ligands CXCL9, 10 and 11. We use biophysical approaches to show that CXCL9, 10 and 11 have very different interactions with extracellular matrix glycosaminoglycans (GAGs) which is exacerbated by specific GAG sulphation. Finally, *in vivo* approaches demonstrate that GAG-binding is critical for CXCL9 driven recruitment of specific T cell subsets (e.g. $CD4^+$) but not others (e.g. $CD8^+$), independent of CXCR3 expression. Our data demonstrate that chemokine expression is complex and that multiple ligands are likely needed for robust leukocyte recruitment across tissues and diseases. We also demonstrate that ECM GAGs facilitate decoding of these complex chemokine signals so that they are either primarily presented on GAG-coated cell surfaces or remain more soluble. Our findings represent a new mechanistic understanding of chemokine mediated immune cell recruitment and identify novel avenues to target specific chemokines during inflammatory disease.

Introduction

Leukocyte migration and recruitment facilitates tissue inflammation which in turn is central to a plethora of diseases such as rheumatoid arthritis, inflammatory bowel disease and cancer(*1*). Leukocyte recruitment is itself primarily driven by chemokines (chemotactic cytokines), making them key players in inflammatory based disease and prime therapeutic targets(*2*). Chemokines are a large family of small proteins that are thought to function by binding to their concomitant receptors on circulating leukocytes(*3*). This interaction produces integrin activation, enabling firm adhesion of leukocytes to the blood vessel wall and subsequent trans-endothelial migration.

Despite their importance the chemokine system has yet to be therapeutically targeted. The reasons for this are multiple, however, a central problem has been the idea of redundancy where multiple chemokine ligands bind to multiple receptors and multiple receptors bind to multiple ligands(*2*, *4*). Several recent studies have set out to determine whether redundancy is a key aspect of chemokine function and have largely demonstrated the opposite, i.e., extreme specificity of the chemokine system(*5–10*). This can be understood from a receptor perspective as recent studies have demonstrated that receptor expression is fine-tuned to have specific receptors on the leukocyte cell surface at each stage of its migration to facilitate specific functions(*9*).

In contrast, when an unbiased analysis is undertaken during inflammatory scenarios a range of different chemokines with over-lapping functions are present in the same location(*8*). This presents a challenge to the idea of specificity of how non-redundant migratory outcomes are produced when multiple ligands for the same receptor are present in the same environment. One mechanistic explanation for this is biased agonism, where different ligands can produce different functional outcomes via the same receptor via different interactions(*11*, *12*). However, this does not fully explain how these specialised functions of chemokines are produced since the differing receptor affinities should in theory dominate which ligands are bound to a receptor at any given time. One way that differential localisation and receptor-binding availability may be achieved is via interactions with extracellular matrix (ECM) glycosaminoglycans (GAGs)(*10*, *13*).

ECM GAGs are particularly present within the glycocalyx that lines the luminal endothelial surface within blood vessels but can also be found throughout tissues(*14*). Chemokine:GAG interactions have been shown to be key for leukocyte recruitment *in vivo* as they facilitate endothelial retention of chemokines on the endothelium in the presence of blood flow(*15*, *16*) and in the case of CXCL4 may directly mediate its function(*17*). However, specific

comprehension of the role of chemokine:GAG interactions on the cell surface and within tissues in leukocyte recruitment is lacking.

Here we show that chemokine ligands and receptors are present in complex, but distinct, families across tissues and disease. These families contain chemokine ligands with over-lapping abilities to recruit the same leukocytes. In particular, the CXCR3 ligands CXCL9, 10 and 11 display over-lapping expression patterns across a wide range of tissues and diseases and have differential roles in recruitment of $CXCR3^+$ cells. We also demonstrate that these ligands have very different interactions with ECM GAGs. These differential interactions facilitate regulation of ligand localisation at the cell surface or in solution. We also found that these interactions play surprisingly specific roles in CXCL9 mediated leukocyte recruitment.

Results

Chemokine ligands and receptors form complex and over-lapping signals

To better understand how chemokines co-ordinate the immune response via leukocyte recruitment we undertook a systematic view of the transcriptional relationship between chemokine ligands and their receptors during inflammation and disease. To do so we analysed transcriptomic data that has been deposited in the EMBL-EBI expression atlas (Fig. 1)(*18*). The database was downloaded followed by minimal "cleaning" of the data to deliberately take an unbiased approach to analysis (Supp. Fig. 1). Output data was then probed using principal component analysis (PCA) and correlation matrix analysis to reveal transcriptional relationships between chemokine ligands and receptors across a range of tissues and diseases in humans and mice (Table 1).

Immediate patterns emerge from this analysis in both the human (Fig. 1 and Supp. Fig. 2) and mouse (Supp. Fig. 3) data, firstly separating into 3 distinct clusters. The largest group, in both the human (cluster 1, Fig. 1A and B) and mouse (cluster 2, Supp. Fig. 3) data, contains a range of genes that have a diverse function in the recruitment of different leukocytes. The other two groups, however, contain genes with closely related functions. The first contains chemokine ligands and receptors that are primarily associated with recruitment of neutrophils are present, specifically CXCL1, CXCL2, CXCL3, CXCL5, CXCL6 and CXCL8 (human cluster 2) and CXCL1, CXCL2, CXCL3, CXCL5 and CCL2 (mouse cluster 1)(*3*). These clusters also contain some additional genes usually associated with recruitment of other cell types, e.g., CCL4 (monocyte) and CCL20 (T cell) in the human data set and CCL2, CCL3, CCL4 and CCL7 (monocyte) in the mouse dataset. Pointedly in both the human and mouse dataset cluster 3 contains CXCL9, CXCL10 and CXCL11 which all signal through CXCR3, primarily in the recruitment of T cells(*19*).

These data demonstrate that chemokine gene expression is associated with specific phases of the immune response so that those genes recruiting the same types of leukocyte are often similarly expressed.

Individual tissues and diseases have specific chemokine ligand and receptor expression patterns

Next we analysed patterns of chemokine ligand and receptor expression more closely by separating the data into different tissues, focussing on the brain (Fig. 1C), lung (Fig. 1D) or lymph node (Fig. 1E). The human (Fig. 1C) and mouse (Supp. Fig. 3) brain data demonstrated clustered expression of neutrophilic chemokines. Human brain cluster 3 contains CXCL1, CXCL2, CXCL3, CXCL5 and CXCL8. Mouse cluster 1 was limited to CXCL1 and CXCL2

alongside a number of monocytic chemokines, suggesting species-specific inflammatory responses in the brain. The clusters in the human lung (Fig. 1D), mouse lung (Supp. Fig. 3C), human lymph node (Fig. 1E), and mouse lymph node (Supp. Fig. 3D) were tissue-specific, but again the close relatedness of the neutrophilic chemokines was maintained.

We next separated the data into diseases for which there were at least ten entries in the expression atlas, namely Crohn's disease, ulcerative colitis, psoriasis, rheumatoid arthritis and Alzheimer's disease (Fig. 2). As above, specific signatures were seen in each context with the first four diseases containing a neutrophilic chemokine cluster. In contrast, the gene relatedness signatures appeared very distinct in the Alzheimer's disease analysis compared to the others, suggesting the chemokine system is functioning differently in this context.

The separation of genes into related clusters was observed across the separated tissues and diseases with specific signatures, reflecting the differential nature of the inflammatory response between tissues and disease. However, certain patterns were clear across these situations, with strikingly consistent clustering of a range of chemokines that can all recruit neutrophils. Strikingly the clustering of CXCL9, CXCL10 and CXCL11 appeared to be present across the separated tissues and diseases.

CXCR3 ligands are consistently expressed together across tissues and disease

Our data thus present a potential example of supposed chemokine redundancy, where CXCL9, 10 and 11, which all bind and signal through CXCR3 (Fig. 3A), may be consistently co-expressed across different inflamed tissues and diseases. To determine the degree of this co-expression we specifically analysed the expression relatedness between the receptor CXCR3 and its ligands CXCL9, 10 and 11 (Fig. 3B and C). This approach confirmed that CXCL9, 10 and 11 are very closely related in expression during inflammation across a range of tissues and

diseases. In contrast, though closely related to each other these ligands have a much lesser transcriptional relationship with their receptor CXCR3 (Fig. 3), suggesting that the ligands and their receptor are usually produced at distinct sites.

This close transcriptional relatedness between ligands but not their receptor is also evident in other families, for example, CXCR1 and 2 and their ligands, where CXCR1 and 2 are also closely transcriptionally related, demonstrating their co-operative function in co-ordinating leukocyte recruitment (Supp. Fig. 4). In contrast, CXCR5, CXCR6, CCR1, CCR4, CCR6, CCR10 are more closely transcriptionally related to their ligands (Supp. Fig. 4-6). Whilst CCR7 and CCR8 have a close transcriptional relationship to one ligand (CCL19 and CCL1, respectively) but not the other (Supp. Fig. 6). These differing relationships may reflect function in local leukocyte positioning, where receptors and ligands would be closely transcriptionally related, versus long range leukocyte recruitment, where they would not be closely related.

CXCL9, 10 and 11 have specific functions *in vivo*

The numerous examples of overlapping expression of CXCL9, 10 and 11 suggests that each is required and thus plays a specific role during the recruitment of $CXCR3^+$ cells. We next confirmed this relatedness at the protein level *in vivo* in the mouse carrageenan inflamed air pouch recruitment model (Fig. 4A and B). The air pouch *in vivo* leukocyte recruitment model was then chosen to determine whether the CXCR3 ligands have a differential function in leukocyte recruitment *in vivo*. We injected equimolar amounts of CXCL9, 10 and 11 into the air pouch (Fig. 4A), allowing analysis of a wide range of leukocytes (Fig. 4C and D and Supp. Fig. 7 and 8). None of the ligands produced statistically significant changes in overall ($CD45^+$) leukocyte recruitment (Fig. 4E) or in the number of neutrophils, macrophages, or eosinophils (Supp. Fig. 9). However, CXCL9 did produce a significant increase in the number of T cells

(TCRβ$^+$) in contrast to CXCL10 and 11 (Fig. 3E) (flow cytometric gating strategy Supp. Fig. 7 and 8). This demonstrates that CXCL9, 10 and 11 do not have the same effect on leukocyte recruitment *in vivo*, supporting previous findings that they each play a specific role in recruitment of T cells(*11*, *19*).

Interactions with ECM GAGs decodes CXCL9, 10 and 11 signals

The data above demonstrate that CXCL9, 10 and 11 are produced in over-lapping combinations and play different roles in T cell recruitment *in vivo*. Therefore, we next sought to understand how these complex chemokine signals could be decoded to allow each to play its specific biological role. We hypothesised that differential interactions with GAG side chains on ECM proteoglycans (Fig. 5A) may produce differential localisation of these ligands within the ECM and on the cell surface.

We utilised bio-layer interferometry (BLI) biophysical analysis to study the interaction between these ligands and isolated GAG sugar models (heparin dp8). BLI demonstrates that CXCL9 (24 ± 12 nM), CXCL10 (253 ± 50 nM) and CXCL11 (520 ± 194 nM) have significantly different GAG affinity estimates (Fig. 5B and C). To analyse chemokine:GAG interactions in a cellular context, binding of labelled CXCL9, CXCL10, and CXCL11 to WT Chinese hamster ovary (CHO) or human embryonic kidney (HEK) cells was performed using flow cytometry (Fig. 5D). In both cases the order of binding (demonstrated by MFI signal) was CXCL9>CXCL10>CXCL11, in agreement with the BLI studies.

To determine which GAGs are responsible for this cellular chemokine binding we used genetically engineered cells that express distinct types of chondroitin sulfate (CS) and heparan sulfate (HS) GAG chains(*20*, *21*). We first compared chemokine binding to WT, CS/HS knock out (KO), CS KO, and HS KO cells derived from CHO and HEK293 cell lines (Fig. 5E).

CXCL9, 10 and 11 all bound to HS on CHO cells since its removal reduced binding, but neither bound to CS since binding was not reduced in its absence. CXCL10 and CXCL11 bound to HS on HEK cells, in contrast CXCL9 binding is only reduced when both HS and CS are removed from HEK cells, suggesting that CXCL9 can bind to both in a potentially redundant fashion.

Oligomerisation has been shown to be key to differential chemokine:GAG interactions (*22*, *23*). Therefore, we next determined the differential oligomerisation of CXCL9, 10 and 11 in the absence and presence of the heparin dp8 GAG using analytical ultracentrifugation (AUC) (Fig. 5F). All three primarily exist as monomers when alone in solution. In the presence of dp8 (ratio 1:2, chemokine:GAG) CXCL9 remains primarily monomeric, CXCL10 becomes 50% dimeric and CXCL11 remains primarily monomeric.

Together these results show that CXCL9, CXCL10 and CXCL11 have a very different ability to bind and be retained on cell surface proteoglycans and will thus be differently distributed within a tissue or on cell surfaces *in vivo*.

GAG fine structure facilitates specificity of binding to CXCL9, CXCL10 and CXCL11

GAG sulphation has previously been shown to drive interaction specificity with other chemokines, e.g., CCL2 and CXCL4(*17*, *24*). We, therefore, hypothesised that GAG sulphation points could produce further differentiation in binding to CXCL9, 10 or 11. GAG sulphation patterns are primarily produced during GAG synthesis by a wide range of different sulfotransferases. Acting on HS are the NDSTs, HS2ST1, HS6STs and HS3STs responsible for N-, 2-O, 6-O, and 3-O sulphation respectively (Fig. 6A)(*25*). Together these modifications can achieve incredible sequence specificity.

In order to dissect their differential contribution to CXCL9, 10 and 11 binding we utilised the recently developed GAGOme cell library, which is a large panel of CHO cells genetically

224 engineered to display distinct GAG features on the cell surfaces (Fig. 6A)(*20*, *26*). Flow
225 cytometry studies revealed that the biggest contributor to HS binding in this context for all
226 three ligands was N-sulfation by NDST1 and 2, unsurprising given that this is the first step in
227 the biosynthetic pathway and essential for priming and modification of different sulfation
228 patterns (Fig. 6B). The effect of HS2ST1 (2-O sulphation) and GLCE (epimerase enhancing
229 levels of 2-O sulphation) removal reduced binding comparably across all three ligands.
230 Combined removal of HS6ST1/2/3 (6-O sulphation) had a much greater effect in reduction of
231 relative binding to CXCL10 and CXCL11 than CXCL9 (Fig. 6B). When absolute rather than
232 relative signal is analysed this difference is exacerbated, in the absence of HS 6-O sulphation
233 the cell surface GAGs have 3 times the capacity to bind CXCL9 compared to CXCL10 and
234 CXCL11 (Fig. 6C).
235 Using the GAGOme approach we also determined the relative effect of 3-O sulphation of HS
236 on binding by using CHO cells in which the different HS3ST isoenzymes responsible for this
237 modification have been knocked-in (KI) (Fig. 6D and E). Adding in 3-O sulphation largely
238 reduced CXCL9 binding, had no significant effect in CXCL10 binding and in some cases
239 reduced CXCL11 binding. There is again evidence of specificity; HS3ST1, HS3ST2,
240 HS3ST3A and HS3ST3B KI cells all have significantly lower binding signal for CXCL9
241 compared to CXCL10 and CXCL11.
242 Given the ability of the GAG sulphation genes to regulate differential binding to chemokines
243 we next sought to determine whether there was a transcriptional relationship between them.
244 We analysed the human expression atlas database from all human tissues pooled for the
245 different GAG synthesis and sulphation genes (Supp. Fig. 10-12). Specifically, analysis of the
246 transcriptional relationship between CXCL9, CXCL10, CXCL11 and the different enzymes
247 that facilitate HS sulphation suggests no positive correlation with the genes facilitating N-, 2-
248 O or 6-O sulphation (Fig. 6F). This may suggest that the chemokine ligands are produced at

distinct times/locations from these sulphation enzymes. In contrast, analysis of the transcriptional relationship between the 3-O sulphation genes and CXCL9, 10 and 11 reveals reasonable correlation of transcription between HS3ST3A and HS3ST3B and these chemokine ligands (Fig. 6F). This suggests that these genes can be expressed at the same time/location and may collaborate to produce specific presentation of CXCL9, CXCL10 and CXCL11.

Global comparison for the GAG synthesis, modification and proteoglycan protein core genes demonstrated less discrete clustering than is the case with chemokine ligand and receptor genes when analysing pooled tissues and diseases (Supp. Fig. 11 and 12). However, more discrete clusters become apparent when the data is separated into specific tissues in both humans and mice.

These data show that in addition to the general interactions with GAGs specific sulphation types can add an additional layer of specificity to these interactions to facilitate differential geographical localisation of ligands that bind to the same receptor.

Interactions with ECM GAGs have a specific role in CXCL9 function *in vivo*

Given the ability of ECM GAGs to bind to CXCL9 and preferentially retain it on the cell surface we next sought to determine whether this interaction is important to its' function *in vivo* (Fig. 6). We first determined which of the cells would be recruited by CXCL9 due to their CXCR3 expression (Fig. 7A and Supp. Fig. 7 and 8). As expected, CXCR3 was present on a number of T cell subsets. Pre-incubation of CXCL9 with purified GAG, to block interaction with endogenous cell surface GAG, inhibited CXCL9 mediated recruitment of $CD4^+$ T cells and possibly TCRγδ cells, but not NK cells or $CD8^+$ cells (Fig. 7B).

These surprisingly specific effects of blocking CXCL9 binding to endogenous GAG suggests that the interaction between CXCL9 and cell surface GAGs plays a vital yet differential role in the recruitment of individual CXCR3$^+$ T cells *in vivo*.

Discussion

Here we show that complex signals of chemokines with over-lapping function can be decoded by ECM GAGs to facilitate specific chemokine localisation during inflammatory disease (Fig. 8). We hypothesise that this differential localisation is critical to the specific function of individual chemokine ligands that has been demonstrated in recent studies(*10*). Alongside these studies, our data may further challenge the classic theory of chemokine redundancy that has been thought to preclude therapeutic targeting of the chemokine system in inflammatory disease(*10*).

Whilst individual papers have presented data showing the presence of multiple chemokine ligands that recruit the same leukocyte, we are not aware of previous unbiased and comprehensive analyses to better define the expression relationship between all chemokine ligands and receptors. Our findings of specific clusters of chemokines and receptors with over-lapping function confirm assumptions that are made about the immune response, which previously have little data to support them. Specifically, given that the early inflammatory response is primed to recruit neutrophils it may not be surprising that we consistently find distinct clusters across tissues and diseases that contain chemokines associated with neutrophil recruitment. Similarly, the consistent overlapping production of the CXCR3 ligands, CXCL9, 10 and 11 may also be unsurprising as there will be distinct stages of the immune response where CXCR3$^+$ T cells are required to fight infection/disease. The fact that in multiple instances chemokines are produced at the same time with supposedly redundant functions supports the

297 idea that each actually performs a specific function in leukocyte recruitment and that multiple
298 chemokine ligands are required to mediate recruitment of a given cell type.
299 The data we present herein of consistently overlapping expression of the CXCR3 ligands
300 presents a fundamental problem to our understanding of chemokine biology. Namely, how
301 would a migrating CXCR3$^+$ T cell be able to interpret a complex signal containing all 3 ligands
302 in the same environment to achieve recruitment and positioning? Our data evidencing the role
303 of ECM GAGs in mediating differential immobilisation of these chemokines on ECM GAGs
304 on the cell surface, and potentially within tissues, may solve this problem. Our data may also
305 explain any potential differences in GAG-mediated protection of chemokines from proteolytic
306 degradation(*27*) and support the idea of targeting GAGs to inhibit CXCL9 function in disease
307 (*16*, *28*, *29*). Overall our data suggest that a CXCR3$^+$ cell is unlikely to encounter these ligands
308 in the same geographical location even with their close transcriptional relationship due to
309 differential GAG binding. This also overcomes the problem whereby if all 3 ligands were
310 present in their soluble form then CXCL11 would dominate binding to CXCR3 due to its much
311 higher affinity for the receptor compared to CXCL9 and 10(*11*).
312 Furthermore, our data revealed that GAG sulphation can add additional layers of specificity to
313 the chemokine:GAG interaction with 6-O sulphation particularly differentiating HS
314 interactions with CXCL9, 10 and 11. The role of HS 3-O sulphation in biology is much less
315 understood than for N-, 2-O or 6-O sulphation due to the problems associated with its
316 analysis(*30*). Strikingly we found that 3-O sulphation mediates differentiation in binding to the
317 CXCR3 ligands and its presence actually reduces binding to CXCL9. Excitingly these data
318 generate the hypothesis that cells and/or tissues may tune their sulphation pattern, e.g., during
319 inflammation, on their ECM GAGs to selectively bind and present certain chemokines over
320 others.

Our study enhances the wider understanding of the co-ordinated role of the chemokine system during inflammation and disease across specific tissues. We also reveal a role for ECM GAGs in decoding the complex chemokine signals that are produced in these contexts to facilitate the specificity of the chemokine system during leukocyte recruitment.

Materials and methods

Materials

Up to 4 mice were housed in cages of up to four in a 12 hr light/dark cycle, with free access to food and water. All experiments were carried out following ethical approval from The University of Manchester and University of Glasgow and under licence from the UK Home Office (Scientific Procedures Act 1986). All chemokines were purchased from Protein Foundry and dp8 and heparin GAGs were purchased from Iduron.

Bioinformatic Analysis

Dataset Construction

To explore gene co-expression, complete microarray and RNA-sequencing differential expression results were downloaded from Expression Atlas in December 2020(*18*). In total, 807 projects (2,450 assays) that operated in *Homo sapiens* and 894 projects (2,431 assays) that operated in *Mus musculus* were selected. Then, accessory description files were used to filter out all tumour-related projects and identify related tissues. In this study, brain, lung, spleen and lymph node were selected.

346 Assay Integration

347 According to literature and preliminary studies, we selected 136 genes that potentially play
348 important roles in chemokine activities during the immune response (*3*). Those 136 genes were
349 categorised into five groups: chemokine ligands (44 genes), chemokine receptors (23 genes),
350 matrix (glycosaminoglycan) synthesis genes (17 genes), matrix metalloproteinase (24 genes),
351 and proteoglycan synthesis (28 genes).

352

353 All analytics results of these 136 genes from tumour-free assays were then collected and
354 concatenated together into one data frame. If the research was forced on a specific organ, only
355 relevant assays were selected. Later, a four-step filtration was carried out to minimise the
356 missing value of each assay but to keep more genes in the data. Firstly, genes that were missed
357 in more than 70% of assays were removed. Secondly, in the output data frame from the last
358 step, assays that contained less than 90% of genes were filtered out. Then, all assays with
359 missing values were cleared. The final output data frame would then be ready for further
360 investigations.

361

362 Co-expression Exploration

363 In order to figure out co-expression relationships between chemokine-related genes, correlation
364 matrixes and principal component analysis (PCA) were plotted. In the correlation matrix,
365 Pearson correlation coefficients between each pair of genes were calculated and visualised as
366 a heatmap using Complex Heatmap package in R (Version 4.1.0)(*31*, *32*). PCA plots were
367 drawn using autoplot package(*33*). Gene cluster results are computed by Clustering Large
368 Applications (CLARA) algorithm(*34*). All plots and correlation tables are available at
369 https://shiny.its.manchester.ac.uk/mqbpryo2/ChemoInt.

370

In vivo leukocyte recruitment assay analysis

Air pouch formation

Air pouches were formed by three subcutaneous injections of 3 ml of sterile air under the dorsal mouse skin every 48 hrs. One day after the final injection the chemokine or carrageenan (1% w/v, Simga-Aldrich) was injected into the air pouch. 24 hrs after injection mice were culled and the air pouch flushed with PBS containing 1% FCS and 1 mM EDTA (two occasions of 3 ml) and analysed for cellular and protein content as below.

Flow cytometry analysis

Post cell isolation, cells were plated at 1 x 10^6 cells per well in v-bottom Nunclon Delta treated 96-well plates (Thermo Fisher Scientific) and washed twice with 100 µl ice-cold 1X PBS to remove proteins in the supernatant before being pelleted by centrifugation at 500 x *g* for 2 min at 4 °C. Cells were then incubated with a Live/Dead amine reactive viability dye (Zombie ultraviolet (UV) dye) (BioLegend) diluted 1:2000 in 10 µl 1X PBS for 15 min at RT in the dark to facilitate dead cell exclusion. Incubation steps were performed in the dark to prevent fluorochrome bleaching.

To prevent non-specific binding of antibodies via Fc receptors on the cell surface, all samples were incubated with FcR block (5 µg ml^{-1} αCD16/CD32 (2.4G2; BD Biosciences)) in 50 μl flow buffer (PBS containing 1% FCS) for 10 min at 4 °C. After blocking, cells were centrifuged at 500 x *g* for 2 min at 4 °C before pelleted cells were resuspended in 50 µl flow buffer containing surface marker antibodies at the dilutions shown in Table 1 for 30 min at 4 °C. Following incubation, cells were washed in 150 µl flow buffer and pelleted by centrifugation at 500 x *g* for 2 min at 4 °C. This wash step was then repeated with a further 200 µl flow buffer. After washing, cells were resuspended in 1% paraformaldehyde (PFA) (Sigma-Aldrich) for 10

min at RT in the dark to prevent the dissociation of antibodies from their target molecules. Cells were then centrifuged at 500 x *g* for 2 min at 4 °C before being resuspended in 200 μl flow buffer ready for acquisition. Cells were stored at 4 °C prior to analysis. In some instances, after blocking, cells were incubated with CXCR3 (1:200) or an IgG isotype control (1:200) in 50 µl flow buffer for 15 min at 37 °C before being washed twice and stained with surface marker antibodies as described above.

To calculate cell counts in some experiments, CountBright Absolute Counting Beads (Thermo Fisher Scientific) were used. Before acquisition of BAL samples on the flow cytometer, 15 µl beads were added per sample. During analysis, beads were identified based on their high side scatter (SSC) and low forward scatter (FSC) phenotype. To calculate absolute cell count, the total number of beads added along with the number of bead events acquired was compared to the volume of cells added and total number of cell events acquired, as per the manufacturers protocol.

tSNE and FlowSOM analysis were performed in R (Version 4.1.3) using CD4, CD8, F4/80, Ly6C, Ter119, CD3, TCRβ, CXCR3, Ly6G, CD11c, B220, CD11b, CD64, Siglec F, NK1.1 and TCRγδ.

Table 1. Flow cytometry antibodies to surface and intracellular markers used to characterize murine samples.

Antigen	Fluorochrome	Clone	Manufacturer	Working Dilution
CXCR3	BV421	CXCR3-173	BioLegend	1:200
IgG Isotype	BV421	HTK88	BioLegend	1:200
CD4	FITC	GK1.5	BD Biosciences	1:200
CD8	PerCP/Cy5.5	53-6.7	BioLegend	1:800

F4/80	APC	BM8	eBioscience	1:200
Ly6C	Af700	HK1.4	BioLegend	1:200
Ter119	APC/ef780	TER-119	eBioscience	1:200
CD3	APC/ef780	17A2	eBioscience	1:100
TCRβ	APC/ef780	H57-597	eBioscience	1:200
Ly6G	BV510	1A8	Biolegend	1:100
CD11c	BV605	N418	BioLegend	1:200
B220	BV650	RA3-6B2	BioLegend	1:100
CD11b	BV711	M1/70	BioLegend	1:800
CD45	BV785	30-F11	BioLegend	1:200
CD64	PE	X54-5/7.1	BioLegend	1:100
SiglecF	PE/CF594	E50-2440	BD Biosciences	1:400
NK1.1	PE/Cy5	PK136	BioLegend	1:200
TCRγδ	PE/Cy7	eBioGL3 (GL-3, GL3)	eBioscience	1:200

415

416

417 ELISA and Luminex analysis of air pouch fluid

418

419 Air-pouch fluid contents were obtained as described in (*8*). Specific concentrations of CXCL9
420 were measured by enzyme-linked immunosorbent assay (ELISA), using the mouse CXCL9
421 ELISA kit (R&D Systems) in a 96-well high binding ELISA plate following the manufacturer's
422 instructions. Plates were read on a VersaMax Microplate Reader (Marshall Scientific) at 450
423 nm. The samples were also analysed using a Bio-Plex Pro Mouse Chemokine Panel, 31- Plex

Assay (Bio-Rad, UK). Samples were read and the data was acquired on a Bio-Plex Manager™ (Software version 6.2).

Chemokine:GAG interaction analysis

Bio-layer interferometry (BLI)

An Octet Red96 system (Sartorius AG, Goettingen, Germany) was used with a methodology adapted from (*22*). GAGs had biotin attached at their reducing end with a previously described approach (*35*) before immobilisation to High Precision Streptavidin (SAX) biosensors (Sartorius AG, Goettingen, Germany). To achieve this SAX biosensors were hydrated for 10 mins in assay buffer (10 mM Hepes, 150 mM NaCl, 3 mM EDTA, 0.05% Tween-20, pH 7.4). Immobilisation of heparin dp8 GAG (0.078 μg/ml) was done in assay buffer until an immobilisation level of approx. 0.1 nm was reached. Sensors were subsequently washed with regeneration buffer (0.1 M Glycine, 1 M NaCl, 0.1% Tween, pH 9.5) and re-equilibrated in assay buffer. Blank reference or GAG coated sensors were then dipped into 200 μL of assay buffer containing chemokines at the indicated concentrations for at least 180 sec (association) before being transferred to assay buffer containing wells (dissociation) for at least 180s before a regeneration buffer wash step. The binding signal was recorded throughout and the signal from binding of chemokine to blank (no immobilised GAG) sensors and by GAG immobilised sensors in assay buffer alone was subtracted. As well as a signal over time, the maximum signal during the association phase of the interaction was recorded and used to generate K_D value esimates in the Octet analysis software. Data were acquired at 5 Hz and analysed using the Octet HT 10.0 analysis programme.

449 Analytical ultra-centrifugation

450 CXCL9, CXCL10 or CXCL11 were re-suspended in PBS to a final concentration of 50 μg/ml
451 either alone or in the presence of heparin dp8 at a ratio of 1:2 (chemokine:GAG). Samples were
452 loaded into 2-sector cells with PBS as a reference and centrifuged at 50,000 rpm in a 4-hole
453 An60Ti rotor monitoring the absorbance at 230 nm until sedimentation was reached. The time-
454 resolved sedimenting boundaries were analysed using Sedfit (*36*). The resulting profiles are
455 shown in Gussi (*37*).

456

457 Cell surface GAG binding

458 This analysis was performed as previously (*20*), using libraries of CHO Glutamine synthetase
459 (GS) -/- or HEK293 6e cells genetically engineered by CRISPR/Cas9 for KO and Zinc finger
460 nucleases for KI of genes(*20*, *21*, *26*). 1×10^5 cells were washed in PBS before incubation with
461 biotinylated recombinant human CXCL9, CXCL10 or CXCL11 (10 μg/mL) (Protein Foundry
462 LLC) in assay buffer (PBS + 1% FBS) for 30 min at 4 °C. Cells were washed with assay buffer
463 followed by incubation with Alexa Fluor 488-streptavidin (1:2000 in assay buffer) (S32354,
464 Invitrogen) for 30 min at 4 °C. Cell were again washed and then re-suspended in assay buffer
465 and fluorescence intensity was analysed using a SA3800 spectral cell analyzer (SONY). All
466 experiments were performed a minimum of three times using triplicate samples.

467

468 **Statistics**

469 Statistical analysis were performed using Prism (GraphPad). Experiments containing two
470 groups were analysed using an unpaired T-test and data containing more than two groups were
471 analysed using a one-way ANOVA with a post-hoc multiple comparison test. $P < 0.05$ was
472 considered to be statistically significant.

473

1. S. Nourshargh, R. Alon, Leukocyte migration into inflamed tissues. *Immunity*. 41, 694–707 (2014).

2. T. J. Schall, A. E. I. Proudfoot, Overcoming hurdles in developing successful drugs targeting chemokine receptors. *Nat Rev Immunol*. 11, 355–363 (2011).

3. F. Bachelerie, A. Ben-Baruch, A. M. Burkhardt, C. Combadière, J. M. Farber, G. J. Graham, R. Horuk, A. H. Sparre-Ulrich, M. Locati, A. D. Luster, A. Mantovani, K. Matsushima, P. M. Murphy, R. Nibbs, H. Nomiyama, C. A. Power, A. E. I. Proudfoot, M. M. Rosenkilde, A. Rot, S. Sozzani, M. Thelen, O. Yoshie, A. Zlotnik, International Union of Basic and Clinical Pharmacology. [corrected]. LXXXIX. Update on the extended family of chemokine receptors and introducing a new nomenclature for atypical chemokine receptors. *Pharmacological Reviews*. 66, 1–79 (2014).

4. A. E. I. Proudfoot, P. Bonvin, C. A. Power, Targeting chemokines: Pathogens can, why can't we? *Cytokine*. 74, 259–267 (2015).

5. J. R. Groom, J. Richmond, T. T. Murooka, E. W. Sorensen, J. H. Sung, K. Bankert, U. H. von Andrian, J. J. Moon, T. R. Mempel, A. D. Luster, CXCR3 chemokine receptor-ligand interactions in the lymph node optimize CD4+ T helper 1 cell differentiation. *Immunity*. 37, 1091–1103 (2012).

6. T. Girbl, T. Lenn, L. Perez, L. Rolas, A. Barkaway, A. Thiriot, C. del Fresno, E. Lynam, E. Hub, M. Thelen, G. Graham, R. Alon, D. Sancho, U. H. von Andrian, M.-B. Voisin, A. Rot, S. Nourshargh, Distinct Compartmentalization of the Chemokines CXCL1 and CXCL2 and the Atypical Receptor ACKR1 Determine Discrete Stages of Neutrophil Diapedesis. *Immunity* (2018), doi:10.1016/j.immuni.2018.09.018.

7. C. Coombs, A. Georgantzoglou, H. A. Walker, J. Patt, N. Merten, H. Poplimont, E. M. Busch-Nentwich, S. Williams, C. Kotsi, E. Kostenis, M. Sarris, Chemokine receptor trafficking coordinates neutrophil clustering and dispersal at wounds in zebrafish. *Nat Commun*. 10, 5166–17 (2019).

8. D. P. Dyer, L. Medina-Ruiz, R. Bartolini, F. Schuette, C. E. Hughes, K. Pallas, F. Vidler, M. K. L. Macleod, C. J. Kelly, K. M. Lee, C. A. H. Hansell, G. J. Graham, Chemokine Receptor Redundancy and Specificity Are Context Dependent. *Immunity*. 50, 378-389.e5 (2019).

9. L. Medina-Ruiz, R. Bartolini, G. J. Wilson, D. P. Dyer, F. Vidler, C. E. Hughes, F. Schuette, S. Love, M. Pingen, A. J. Hayes, J. Fu, A. F. Stewart, G. J. Graham, Analysis of combinatorial chemokine receptor expression dynamics using multi-receptor reporter mice. *Elife*. 11, e72418 (2022).

10. D. P. Dyer, Understanding the mechanisms that facilitate specificity, not redundancy, of chemokine mediated leukocyte recruitment. *Immunology*. 290, 21292 (2020).

11. M. Metzemaekers, V. Vanheule, R. Janssens, S. Struyf, P. Proost, Overview of the Mechanisms that May Contribute to the Non-Redundant Activities of Interferon-Inducible CXC Chemokine Receptor 3 Ligands. *Front Immunol*. 8, 1970 (2017).

513 12. A. Steen, O. Larsen, S. Thiele, M. M. Rosenkilde, Biased and g protein-independent
514 signaling of chemokine receptors. *Front Immunol*. 5, 277 (2014).

515 13. T. M. Handel, D. P. Dyer, Perspectives on the Biological Role of
516 Chemokine:Glycosaminoglycan Interactions. *J Histochem Cytochem*, 22155420977971
517 (2020).

518 14. A. L. Gray, N. Pun, A. J. L. Ridley, D. P. Dyer, Role of extracellular matrix
519 proteoglycans in immune cell recruitment. *Int J Exp Pathol* (2022), doi:10.1111/iep.12428.

520 15. A. E. I. Proudfoot, T. M. Handel, Z. Johnson, E. K. Lau, P. LiWang, I. Clark-Lewis, F.
521 Borlat, T. N. C. Wells, M. H. Kosco-Vilbois, Glycosaminoglycan binding and
522 oligomerization are essential for the in vivo activity of certain chemokines. *Proc Natl Acad*
523 *Sci USA*. 100, 1885–1890 (2003).

524 16. H. Crijns, V. Vanheule, P. Proost, Targeting Chemokine—Glycosaminoglycan
525 Interactions to Inhibit Inflammation. *Front Immunol*. 11, 907 (2020).

526 17. A. L. Gray, R. Karlsson, A. R. Roberts, A. J. Ridley, N. Pun, C. Hughes, L. Medina-Ruiz,
527 H. L. Birchenough, C. L. Salanga, E. A. Yates, J. E. Turnbull, T. M. Handel, G. J. Graham,
528 T. A. Jowitt, I. Schiessl, R. P. Richter, R. L. Miller, D. P. Dyer, Chemokine CXCL4
529 interactions with extracellular matrix proteoglycans mediate wide-spread non-receptor
530 mediated immune cell recruitment. *Biorxiv*, in press, doi:10.1101/2022.07.10.499282.

531 18. R. Petryszak, M. Keays, Y. A. Tang, N. A. Fonseca, E. Barrera, T. Burdett, A. Füllgrabe,
532 A. M.-P. Fuentes, S. Jupp, S. Koskinen, O. Mannion, L. Huerta, K. Megy, C. Snow, E.
533 Williams, M. Barzine, E. Hastings, H. Weisser, J. Wright, P. Jaiswal, W. Huber, J.
534 Choudhary, H. E. Parkinson, A. Brazma, Expression Atlas update—an integrated database of
535 gene and protein expression in humans, animals and plants. *Nucleic Acids Res*. 44, D746–
536 D752 (2016).

537 19. J. R. Groom, A. D. Luster, CXCR3 ligands: redundant, collaborative and antagonistic
538 functions. *Immunol Cell Biol*. 89, 207–215 (2011).

539 20. Y.-H. Chen, Y. Narimatsu, T. M. Clausen, C. Gomes, R. Karlsson, C. Steentoft, C. B.
540 Spliid, T. Gustavsson, A. Salanti, A. Persson, A. Malmström, D. Willén, U. Ellervik, E. P.
541 Bennett, Y. Mao, H. Clausen, Z. Yang, The GAGOme: a cell-based library of displayed
542 glycosaminoglycans. *Nat Methods*. 15, 881–888 (2018).

543 21. Y. Narimatsu, H. J. Joshi, R. Nason, J. V. Coillie, R. Karlsson, L. Sun, Z. Ye, Y.-H.
544 Chen, K. T. Schjoldager, C. Steentoft, S. Furukawa, B. A. Bensing, P. M. Sullam, A. J.
545 Thompson, J. C. Paulson, C. Büll, G. J. Adema, U. Mandel, L. Hansen, E. P. Bennett, A.
546 Varki, S. Y. Vakhrushev, Z. Yang, H. Clausen, An Atlas of Human Glycosylation Pathways
547 Enables Display of the Human Glycome by Gene Engineered Cells. *Mol Cell*. 75, 394-407.e5
548 (2019).

549 22. D. P. Dyer, C. L. Salanga, B. F. Volkman, T. Kawamura, T. M. Handel, The dependence
550 of chemokine-glycosaminoglycan interactions on chemokine oligomerization. *Glycobiology*.
551 26, 312–326 (2016).

552 23. D. P. Dyer, E. Migliorini, C. L. Salanga, D. Thakar, T. M. Handel, R. P. Richter,
553 Differential structural remodelling of heparan sulfate by chemokines: the role of chemokine
554 oligomerization. *Open Biol*. 7, 160286 (2017).

555 24. R. L. Miller, A. B. Dykstra, W. Wei, C. Holsclaw, J. E. Turnbull, J. A. Leary, Enrichment
556 of Two Isomeric Heparin Oligosaccharides Exhibiting Different Affinities toward Monocyte
557 Chemoattractant Protein-1. *Anal. Chem*. 88, 11551–11558 (2016).

558 25. D. Xu, J. D. Esko, Demystifying heparan sulfate-protein interactions. *Annu. Rev.*
559 *Biochem*. 83, 129–157 (2014).

560 26. R. Karlsson, P. Chopra, A. Joshi, Z. Yang, S. Y. Vakhrushev, T. M. Clausen, C. D.
561 Painter, G. P. Szekeres, Y.-H. Chen, D. R. Sandoval, L. Hansen, J. D. Esko, K. Pagel, D. P.
562 Dyer, J. E. Turnbull, H. Clausen, G.-J. Boons, R. L. Miller, Dissecting structure-function of
563 3-O-sulfated heparin and engineered heparan sulfates. *Sci Adv*. 7, eabl6026 (2021).

564 27. M. Metzemaekers, A. Mortier, R. Janssens, D. Boff, L. Vanbrabant, N. Lamoen, J. V.
565 Damme, M. M. Teixeira, I. D. Meester, F. A. Amaral, P. Proost, Glycosaminoglycans
566 Regulate CXCR3 Ligands at Distinct Levels: Protection against Processing by Dipeptidyl
567 Peptidase IV/CD26 and Interference with Receptor Signaling. *Int J Mol Sci*. 18, 1513 (2017).

568 28. V. Vanheule, D. Boff, A. Mortier, R. Janssens, B. Petri, E. Kolaczkowska, P. Kubes, N.
569 Berghmans, S. Struyf, A. J. Kungl, M. M. Teixeira, F. A. Amaral, P. Proost, CXCL9-Derived
570 Peptides Differentially Inhibit Neutrophil Migration In Vivo through Interference with
571 Glycosaminoglycan Interactions. *Front Immunol*. 8 (2017), doi:10.3389/fimmu.2017.00530.

572 29. V. Vanheule, R. Janssens, D. Boff, N. Kitic, N. Berghmans, I. Ronsse, A. J. Kungl, F. A.
573 Amaral, M. M. Teixeira, J. V. Damme, P. Proost, A. Mortier, The positively charged
574 COOH-terminal glycosaminoglycan binding CXCL9(74-103) peptide inhibits CXCL8-
575 induced neutrophil extravasation and monosodium urate crystal-induced gout in mice. *J Biol*
576 *Chem*., in press, doi:10.1074/jbc.m115.649855.

577 30. B. E. Thacker, D. Xu, R. Lawrence, J. D. Esko, Heparan sulfate 3-O-sulfation: a rare
578 modification in search of a function. *Matrix Biol*. 35, 60–72 (2014).

579 31. J. Benesty, J. Chen, Y. Huang, I. Cohen, Noise Reduction in Speech Processing. *Springer*
580 *Top Signal Process*, 1–4 (2009).

581 32. Z. Gu, R. Eils, M. Schlesner, Complex heatmaps reveal patterns and correlations in
582 multidimensional genomic data. *Bioinformatics*. 32, 2847–2849 (2016).

583 33. Y. Tang, M. Horikoshi, W. Li, ggfortify: Unified Interface to Visualize Statistical Results
584 of Popular R Packages. *R J*. 8, 474 (2016).

585 34. L. Kaufman, P. J. Rousseeuw, Finding Groups in Data. *Wiley Ser Probab Statistics*
586 (2018), doi:10.1002/9780470316801.

587 35. D. Thakar, E. Migliorini, L. Coche-Guerente, R. Sadir, H. Lortat-Jacob, D. Boturyn, O.
588 Renaudet, P. Labbe, R. P. Richter, A quartz crystal microbalance method to study the

589 terminal functionalization of glycosaminoglycans. *Chem. Commun. (Camb.)*. 50, 15148–
590 15151 (2014).

591 36. P. Schuck, Size-distribution analysis of macromolecules by sedimentation velocity
592 ultracentrifugation and lamm equation modeling. *Biophys J*. 78, 1606–1619 (2000).

593 37. C. A. Brautigam, Calculations and Publication-Quality Illustrations for Analytical
594 Ultracentrifugation Data. *Meth Enzymol*. 562, 109–133 (2015).

595

596

Figure. 1

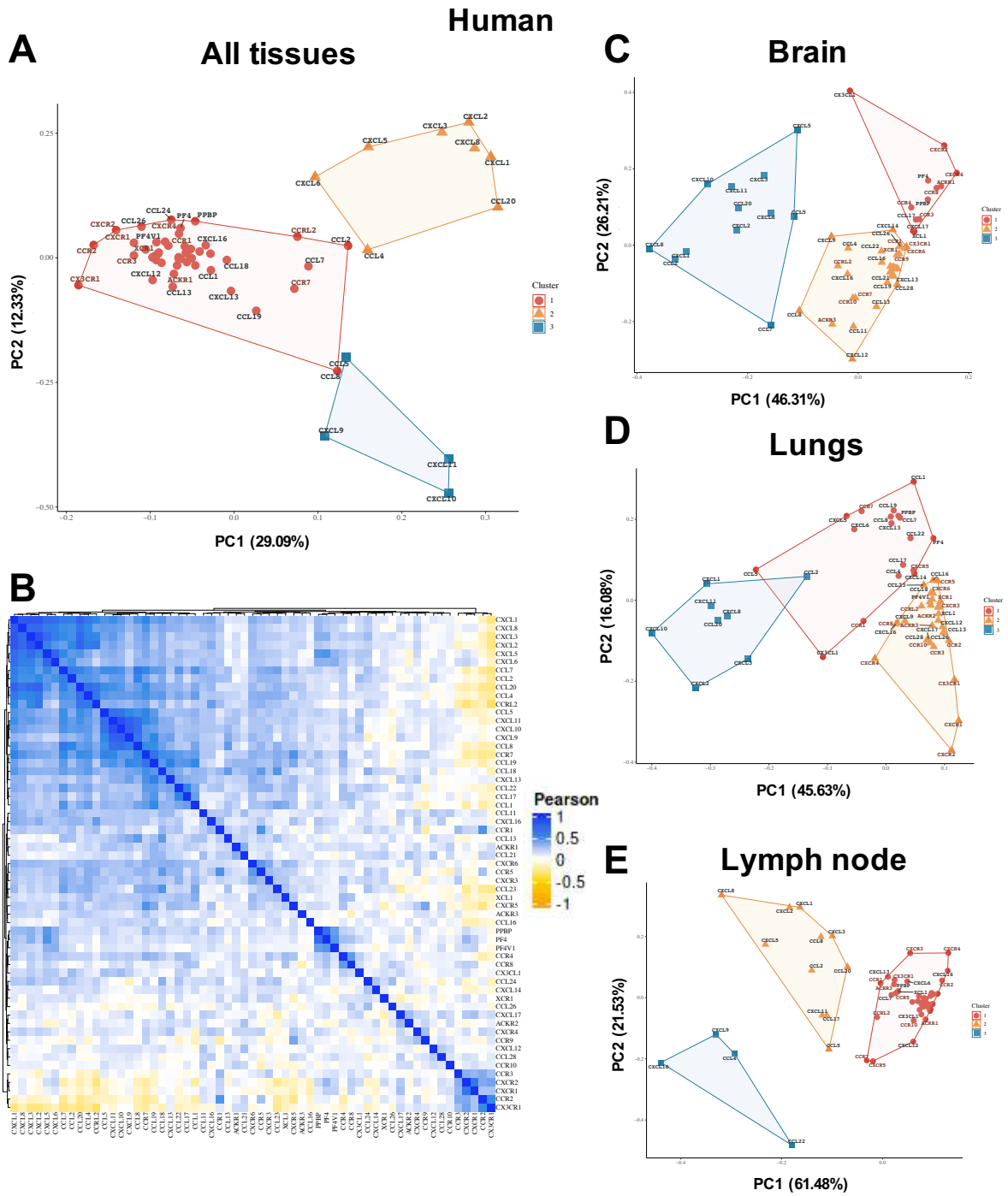

597

598

599 **Figure 1. Chemokine receptors and ligands are present in complex and tissue specific**
600 **patterns during inflammation.** The EMBL-ELI expression atlas was analysed for relatedness
601 on expression of all chemokine ligands and receptors in human data from (A) PCA analysis,
602 (B) heat map analysis of all data pooled or separated into PCA analysis of (C) brain, (D) lungs
603 or (E) lymph node.
604

Figure. 2

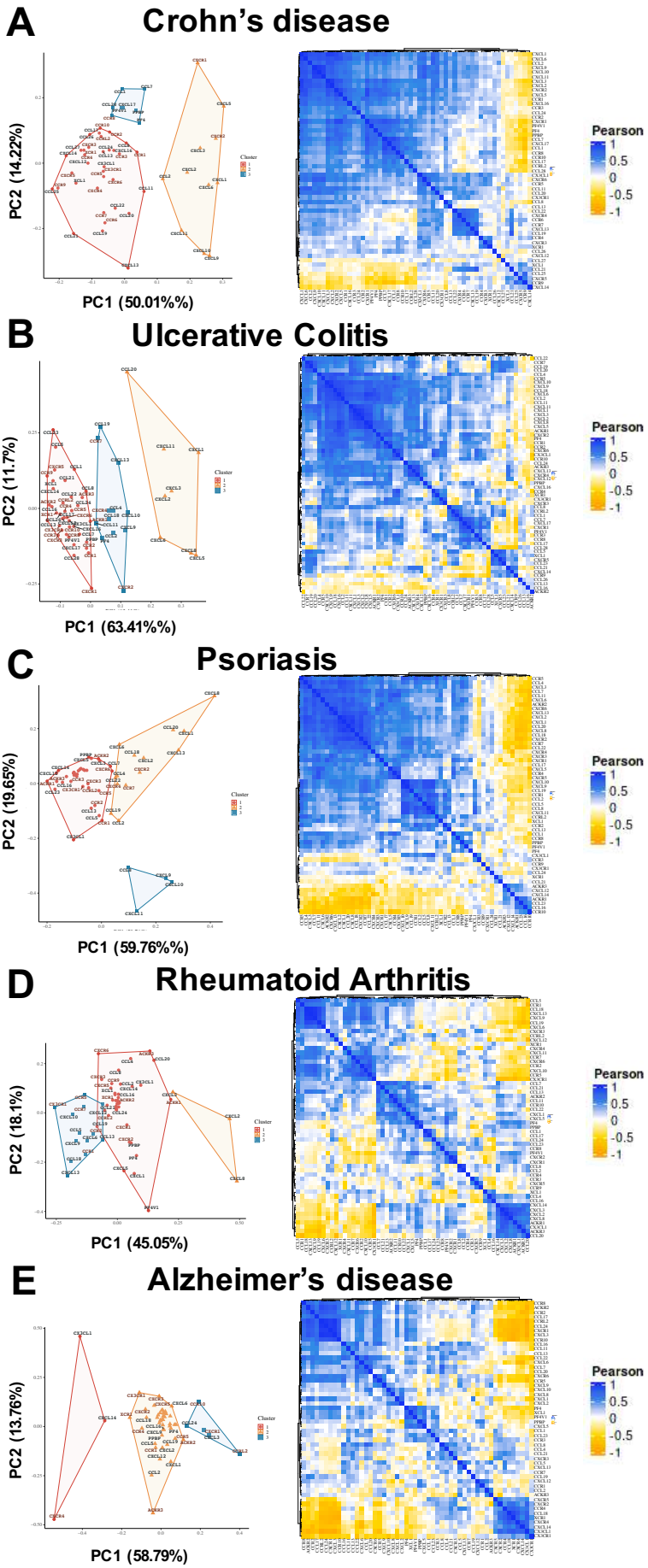

606 **Figure 2. Chemokine receptors and ligands are present in disease specific patterns.** The
607 EMBL-ELI expression atlas was analysed for relatedness on expression of all chemokine
608 ligands and receptors in human data from (A) Crohn's disease (B) ulcerative colitis, (C)
609 psoriasis, (D) rheumatoid arthritis and (E) Alzheimer's disease.
610

Figure. 3

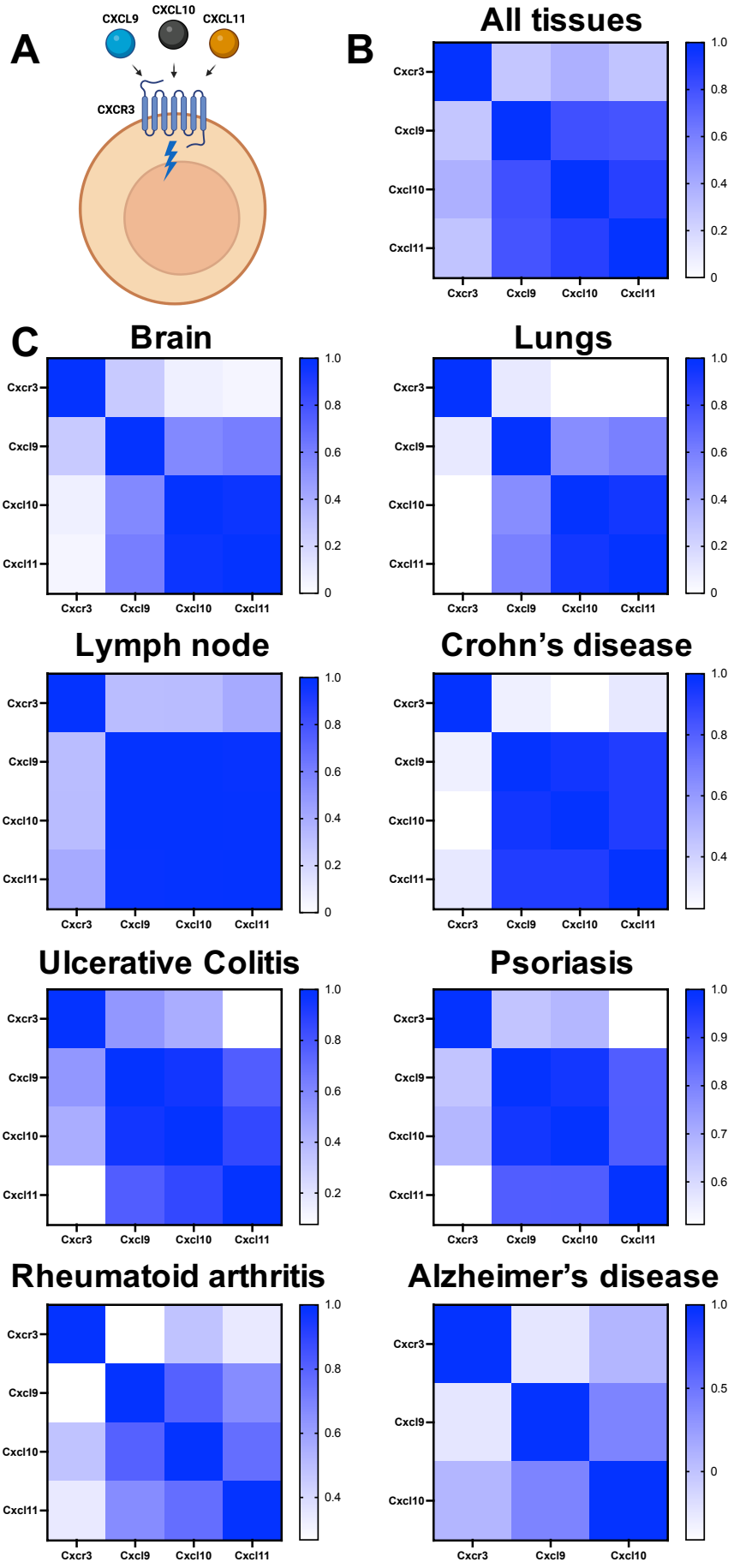

612 **Figure 3. The CXCR3 ligands CXCL9, 10 and 11 are expressed in over-lapping patterns**
613 **across tissues and disease.** (A) CXCL9, 10 and 11 can all bind and signal through the
614 chemokine receptor CXCR3 that is typically found on T cells. (B) The EMBL-ELI expression
615 atlas (human) was analysed for relatedness in expression of CXCR3 and its' ligands CXCL9,
616 10 and 11 across all tissues or (C) in distinct tissues and diseases.
617

Figure. 4

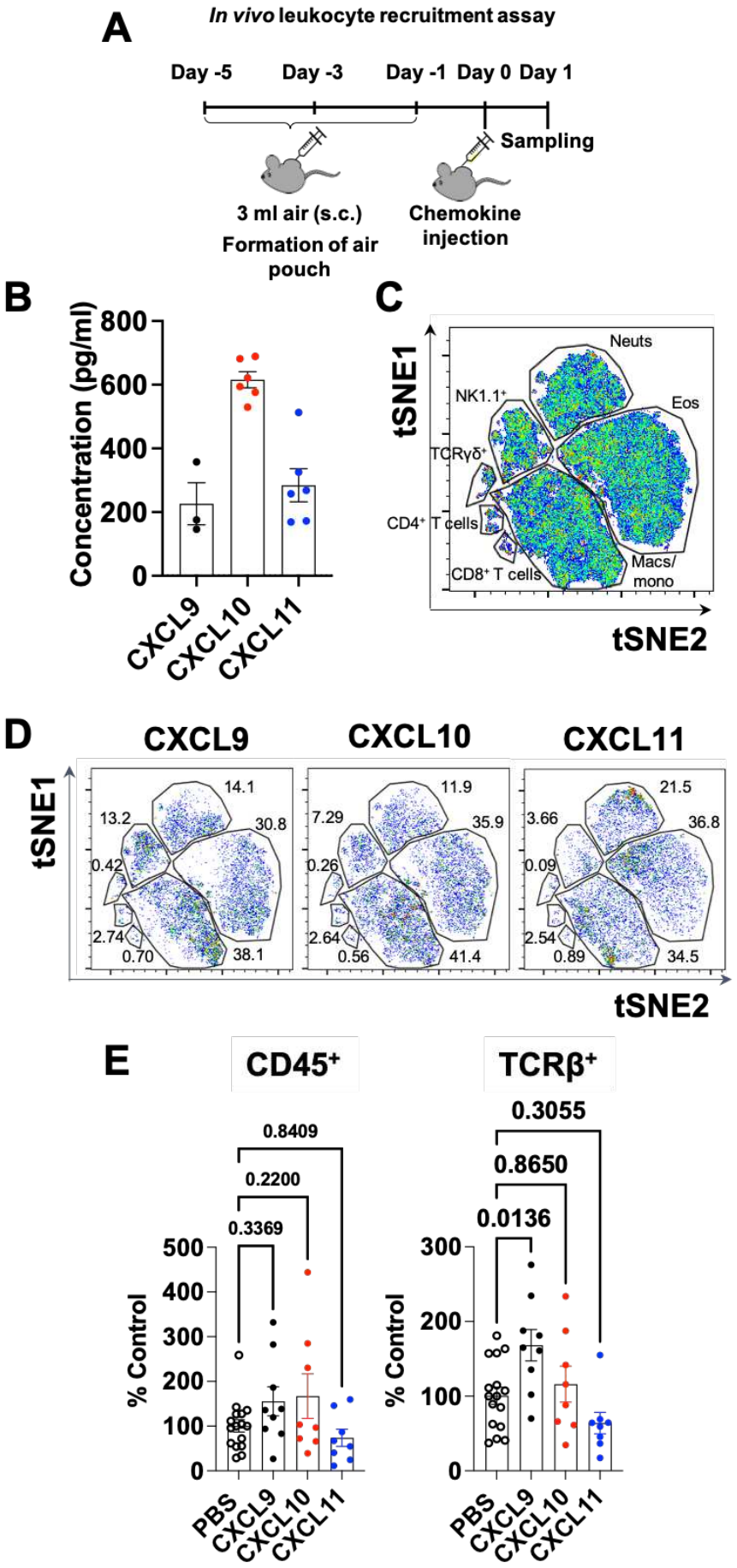

Figure 4. CXCL9, 10 and 11 have different abilities to mediate cell recruitment *in vivo*. (A) Schematic of the *in vivo* air pouch leukocyte recruitment model. (B) Analysis of chemokine concentration in the carrageenan inflamed air pouch. (C) Representative tSNE of all murine cells gated on live, single, $CD45^+$ and built on CD4, CD8, F4/80, Ly6C, Ter119, CD3, TCRβ, CXCR3, Ly6G, CD11c, B220, CD11b, CD64, Siglec F, NK1.1 and TCRγδ. FlowSOM clusters are illustrated by gates. (D) tSNE analysis of air pouches injected with equimolar amounts of CXCL9, 10 and 11. (E) Quantification of all leukocytes ($CD45^+$) and T cells within the air pouch following injection of CXCL9, 10 or 11. E analysed using a one-way ANOVA.

Figure. 5

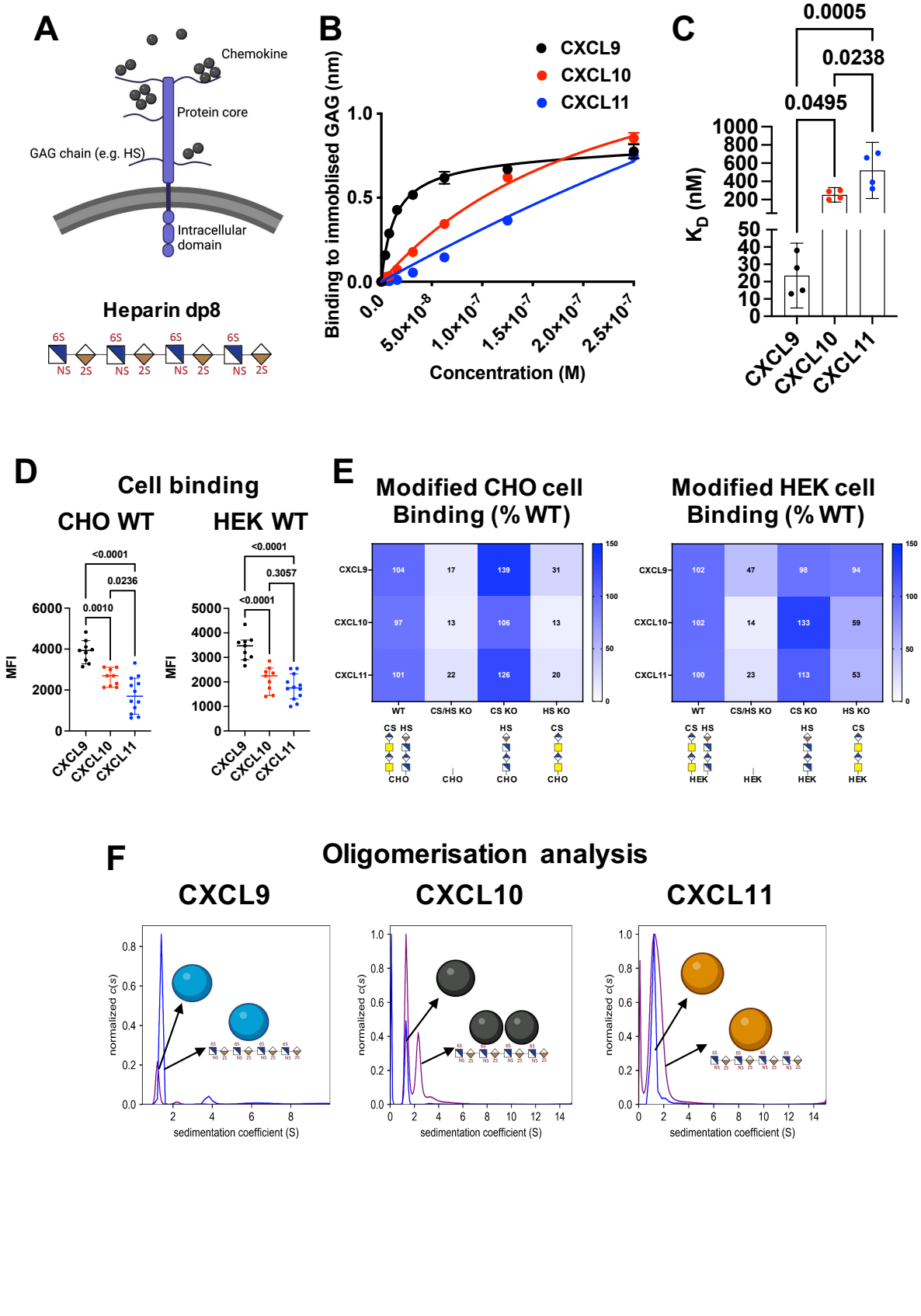

628

629

Figure 5. CXCL9, 10 and 11 have different affinity interactions with ECM GAGs. (A) GAGs are sugar side chains found on cell surface and ECM proteoglycans and purified dp8 can be used as a model GAG. (B) Immobilised dp8 binding to chemokines in BLI equilibrium signal is plotted against chemokine concentration. (C) BLI data in B was analysed for steady state affinity (K_D) estimates. (D) Binding of biotin-labelled chemokines to WT CHO and HEK293 cells quantified by mean fluorescent intensity (MFI) detected using flow cytometry. (E) Binding of biotin-labelled chemokines to genetically modified CHO cells with KO of B4galt7 (CS/HS KO), CSgalnact1/2/Chsy1 (CS KO) and Extl3 (HS KO), and HEK293 cells with KO of B4GALT7 (CS/HS KO), CHSY1/3 (CS KO), and EXTL3 (HS KO). All data was normalized to MFI for WT. (F) AUC analysis of chemokine oligomerization state in the absence and presence of heparin dp8 GAG. Data plotted ± SEM, (B) is representative of two separate experiments, (C) is pooled data from two separate experiments, (D) contains data from three separate pooled experiments, (E) is the mean of three separate pooled experiments and (F) is representative of two separate experiments. C and D analysed using a one-way ANOVA.

Figure. 6

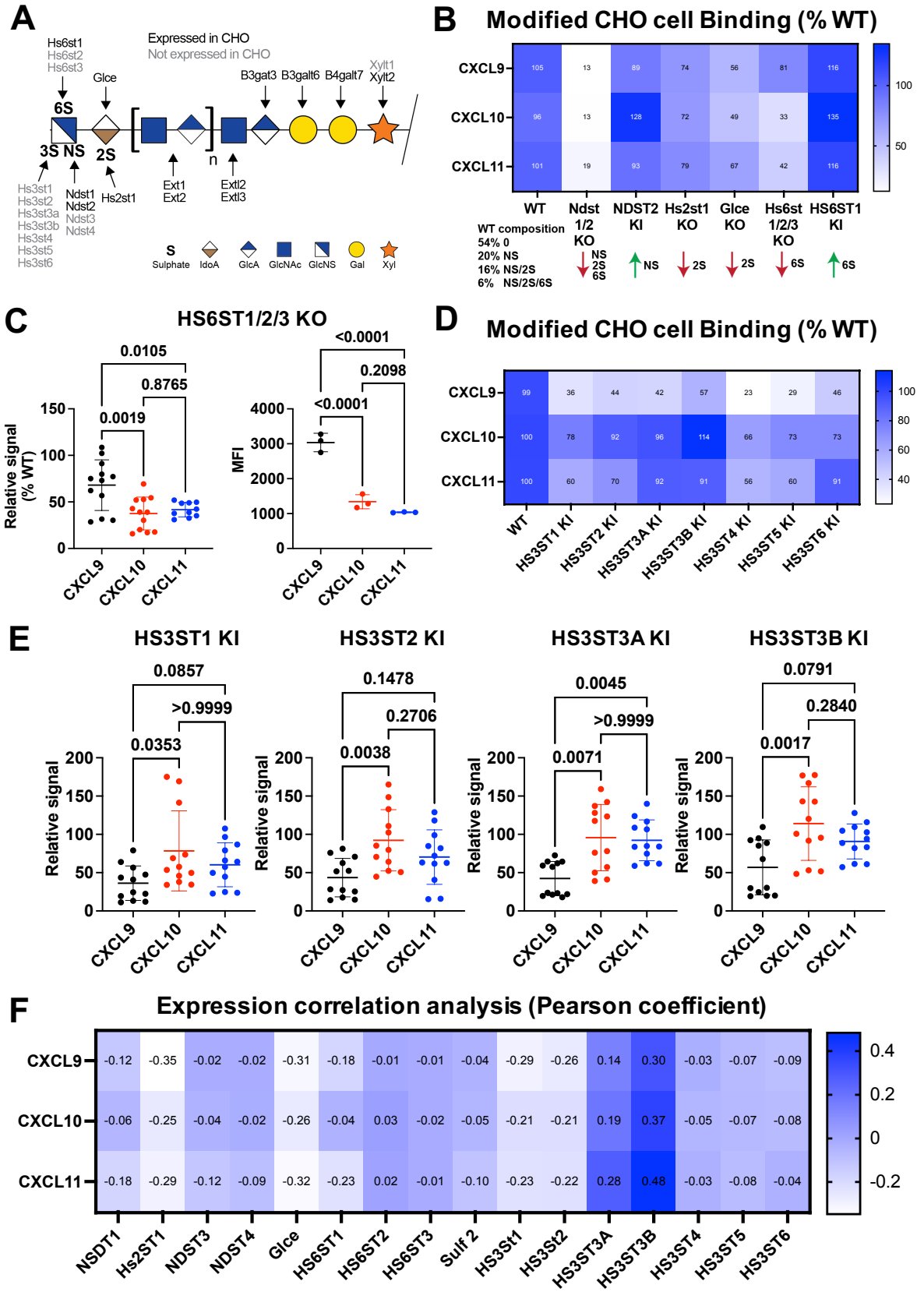

645

Figure 6. ECM GAG sulphation mediates differentiation of binding to CXCL9, 10 and 11. (A) Schematic of HS GAG structure, including sulphation points and the enzymes that produce them. (B) Normalised (relative to wild type) binding of labelled CXCL9, 10 or 11 to genetically modified CHO cells. (C) Normalised and absolute binding of CXCL9, 10 and 11 to CHO cells in which KS^ST1/2/3 have been genetically removed. (D and E) Normalised binding of CXCL9, 10 and 11 to CHO cells genetically engineered to express the enzymes regulating 3-O GAG sulphation. (F) EMBL-ELI expression atlas analysis of relatednessCXCL9, 10 and 11 and GAG sulphation gene expression. B and D, data plotted as mean from three separate pooled experiments. C and E data plotted as mean ± SEM from three separate pooled experiments and analysed using a one-way ANOVA.

Figure. 7

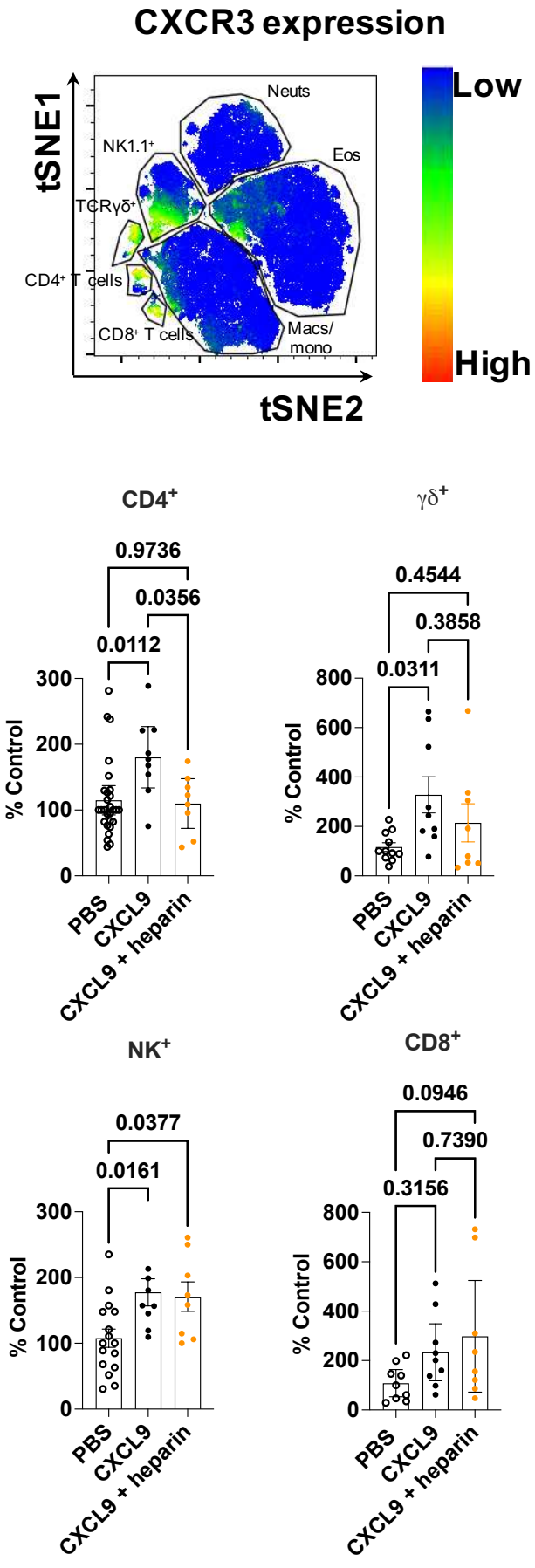

Figure 7. CXCL9:GAG interaction plays specific roles in mediating recruitment of different CXCR3^{+} cells. (A) Representative tSNE analysis of CXCR3 expression of chemokine recruited leukocytes gated on live, single, CD45^{+} and built on CD4, CD8, F4/80, Ly6C, Ter119, CD3, TCRβ, CXCR3, Ly6G, CD11c, B220, CD11b, CD64, Siglec F, NK1.1 and TCRγδ. (B) Normalised leukocyte counts of air pouches injected with the indicated solutions. (B) Data expressed ± SEM from three pooled separate experiments analysed using a one-way ANOVA.

Figure. 8

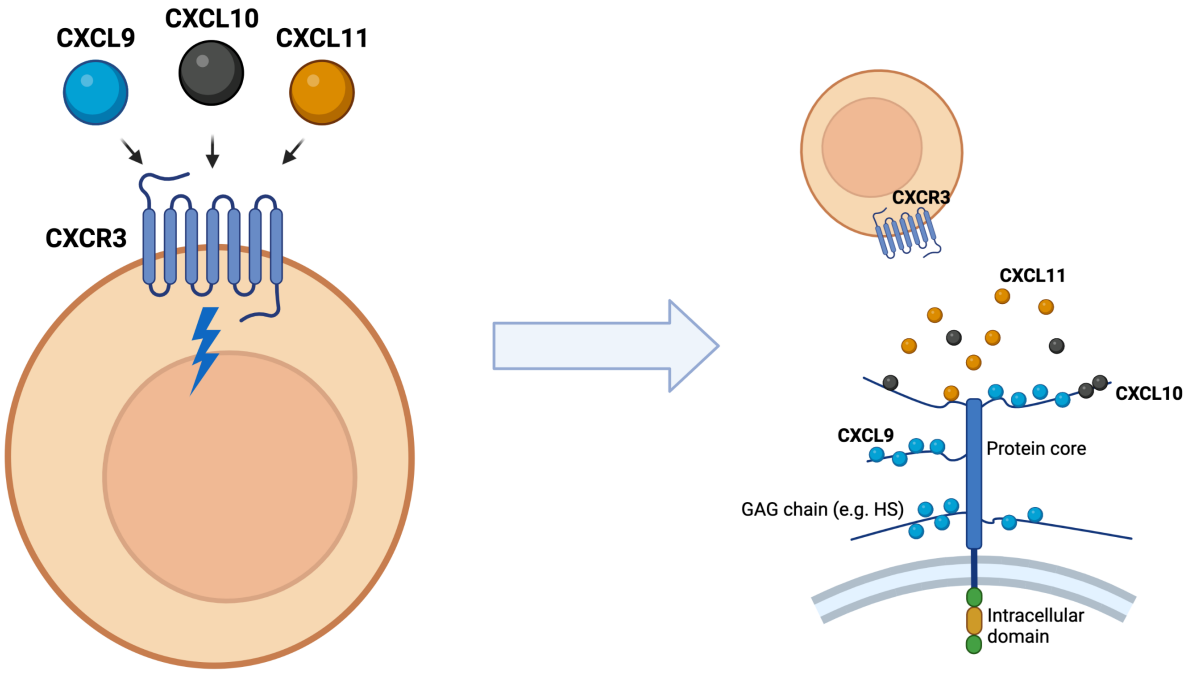

Figure 8. Complex chemokine signals are "decoded" via interactions with ECM GAGs. (A) CXCL9, 10 and 11 all bind to the same receptor with different affinities and biased signalling outcomes and are found in over-lapping expression patterns during inflammation and disease. (B) Differential GAG interactions means that CXCL9 is more likely to be retained on GAGs on the cell surface or within the ECM, with CXCL10 and CXCL11 being more likely to be present in their soluble state.